Available online at www.sciencedirect.com
ScienceDirect
International Journal of Multiphase Flow 34 (2008) 905–915
International Journal of Multiphase Flow
www.elsevier.com/locate/ijmulflow

Experimental investigation of the onsets of gas and liquid entrainment from a small branch mounted on an inclined wall

J.T. Bartley, H.M. Soliman *, G.E. Sims

Department of Mechanical and Manufacturing Engineering, University of Manitoba, 15 Gillson Street, Winnipeg, Man., Canada R3T 5V6

Received 2 November 2007; received in revised form 23 April 2008
Available online 6 June 2008

Abstract

The phenomena of the onsets of liquid entrainment and gas entrainment were investigated experimentally for the case of a flat plane with a circular outlet branch of diameter d (=6.35 mm) at the plane centre. This flat plane was situated in a large tank containing a stratified mixture of air and water under pressure (317 kPa for most experiments and 520 kPa for a few experiments) and at room temperature. The plane was inclined through various angles (θ) in increments of 30°, from the outlet branch orientation being vertically upward through the horizontal to vertically downward. For both onsets the vertical distance between the centre of the outlet branch and the undisturbed gas–liquid interface (h) was measured for various angles of inclination and Froude numbers. Both onsets were observed visually through a large viewing part of the test section. It was found that for both onsets there is a range of inclination angles where the onset h depended on θ and a range where the onset h essentially did not depend on θ. The data were correlated in terms of onset h/d, Froude number, and θ where there was dependence of onset h on the angle of inclination.

Keywords: Onset of liquid entrainment; Onset of gas entrainment; Small branch; Inclined wall; Flow phenomena; Experimental data; Empirical correlation

1. Introduction

The development of empirical correlations and theoretical models for the accurate prediction of the mass flow rate and quality during two-phase discharge through small branches mounted on walls and large pipes has received considerable attention in the literature due to the relevance of this topic to many industrial applications. Examples of these applications include the flow through small breaks in the horizontal cooling channels of nuclear reactors during postulated loss-of-coolant accidents; the flow distribution in the CANDU (Canadian Deuterium and Uranium reactors) header-feeder system during accident scenarios; and two-phase distribution systems in general, where a certain incoming two-phase stream fed into a large header or chamber is divided among a number of discharging streams, as for instance, in a shell-and-tube heat exchanger. Knowledge of the pertinent flow phenomena, as well as the mass flow rate and quality of all discharging streams is important for the design and performance prediction of such systems.

Zuber (1980) considered the case of a single discharge from a large pipe containing a stratified two-phase mixture through a small branch mounted on the pipe wall. He pointed out that two distinct phenomena may occur, depending on the location of the gas–liquid interface relative to the branch inlet. If the interface is located above the branch inlet, gas can be entrained (by vortex or vortex-free motion) into the predominantly liquid flow through the branch. On the other hand, if the interface is located below the branch inlet, liquid may be entrained into the predominantly gas flow. Zuber proposed simplified correlations for the onsets of these phenomena in terms of flow and system parameters for three branch locations on the pipe's circumference, namely top, bottom and side.

* Corresponding author. Tel.: +1 204 474 9307; fax: +1 204 275 7507.
E-mail address: hsolima@cc.umanitoba.ca (H.M. Soliman).

0301-9322/$ - see front matter © 2008 Elsevier Ltd. All rights reserved.
doi:10.1016/j.ijmultiphaseflow.2008.04.003

Later, detailed experiments were reported on the onsets of gas and liquid entrainment from a large stratified region through a single branch (e.g., Smoglie and Reimann, 1986; Schrock et al., 1986; Yonomoto and Tasaka, 1988, 1991; Micaelli and Memponteil, 1989; Reimann and Khan, 1984; Hassan et al., 1998; Welter et al., 2004). These investigations considered one or more of the following branch orientations: horizontal, vertical-up, and vertical-down.

In a recent publication, Lee et al. (2007) investigated the onsets of gas and liquid entrainment in a single inclined branch attached to a horizontal header. The experiment was conducted with two branch diameters of 16.0 and 24.8 mm and one header of 184-mm inner diameter. Data for the onset of liquid entrainment (OLE) were obtained for upward inclination angles of the branch of 0°, 30°, 45°, 60°, and 90° (measured from the horizontal), while for the onset of gas entrainment (OGE), the data corresponded to downward inclination angles of the branch of 0°, 30°, 45°, 60°, and 90° (measured from the horizontal). A comparison between the results of Lee et al. and the present results is given later in this paper.

To the best of the authors' knowledge, the experimental data of Lee et al. (2007) is the only set currently available on the OLE and OGE through inclined branches mounted on a circular wall. Keeping in mind that small breaks may occur at any location around the circumference of a pipe or a flat retaining wall of a header, we note the need for more data on the conditions for OLE and OGE through branches mounted on inclined walls. In the present investigation, the phenomena of OLE and OGE will be considered for branches mounted on a flat wall with upward and downward inclination angles of the wall for both onsets and cover the range of inclinations from vertical upward to vertical downward branches. New flow phenomena and trends that were not noted by previous authors were observed in the present study. The objectives of this investigation were to generate experimental data on the conditions for the onsets, to examine the pertinent flow phenomena, and to correlate the experimental data.

2. Experimental investigation

2.1. Experimental parameters

The independent parameters that are relevant to this experimental investigation are shown schematically in Fig. 1(a) and (b). A discharge branch of diameter d is mounted on a wall in contact with a stratified gas–liquid mixture at stagnation pressure and temperature P_o and T_o, respectively. The wall is inclined an angle θ from the vertical direction. The angle θ is considered positive if the wall is inclined away from the interface as viewed from the gas side (Fig. 1a) and negative if the wall is inclined towards the interface as viewed from the gas side (Fig. 1b). The point of intersection between the plane of the wall and the centreline of the branch is used as a reference point for measuring the vertical distance to the gas–liquid interface, which is designated as h. The value of h is positive when the interface is above the reference point and negative when the interface is below the reference point. Discharging flow through the branch is directed (via a connecting line) to a separator where the pressure is maintained at P_s. The mass flow rate through the branch is controlled by the pressure difference ΔP, where $\Delta P = P_o - P_s$.

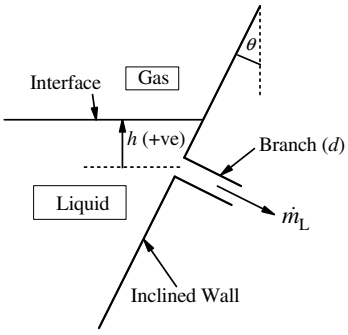

(a) Example of positive h and positive θ

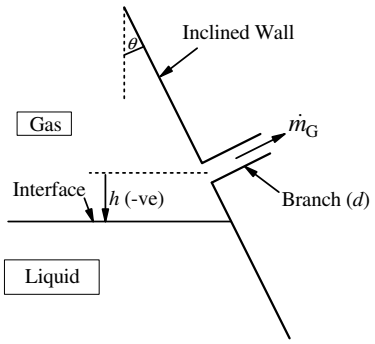

(b) Example of negative h and negative θ

Fig. 1. Schematic showing independent parameters.

For the condition of fixed P_o, T_o, and ΔP, let us consider the dependence of the flow discharge on h. At high positive values of h, the flow discharge will be in the form of single-phase liquid and the flow rate, $\dot{m}_L$, would be essentially independent of h for the large values of ΔP considered in this experiment. On decreasing h, a critical value is reached where gas begins being entrained in the liquid flow. This condition is called the OGE at which $h = h_{OGE}$ and $\dot{m}_L = \dot{m}_{L,OGE}$. A further decrease in h results in a two-phase discharge with an expected decrease in the total mass flow rate through the branch. On the other hand, starting from a high negative value of h, single-phase gas flows through the branch at a rate of $\dot{m}_G$. On decreasing $|h|$, i.e., on raising the interface, a critical condition is reached where liquid begins being entrained in the gas flow (OLE) and thus, $h = h_{OLE}$, and $\dot{m}_G = \dot{m}_{G,OLE}$.

It is useful to cast the experimental data in terms of dimensionless quantities in order to facilitate the correlation. The dimensionless groups that are important to this investigation are the critical interface heights normalized with respect to the branch diameter, h_{OGE}/d and $|h_{OLE}|/d$, and the ratio of inertia forces to gravity forces in the flow

which is expressed by the Froude number, Fr. For the cases of OLE and OGE, the relevant Froude numbers Fr_G and Fr_L, respectively, were defined as

$$Fr_G \equiv \frac{(4/\pi)\dot{m}_{G,OLE}}{\sqrt{gd^5\rho_G(\rho_L-\rho_G)}}, \quad (1)$$

and

$$Fr_L \equiv \frac{(4/\pi)\dot{m}_{L,OGE}}{\sqrt{gd^5\rho_L(\rho_L-\rho_G)}},$$

where g is the gravitational acceleration, ρ_G and ρ_L are the gas and liquid densities, respectively. Developing the functional relationships, $h_{OGE}/d = f_1(Fr_L,\theta)$ and $|h_{OLE}|/d = f_2(Fr_G,\theta)$, was one of the main objectives of the present study.

2.2. Experimental apparatus

A schematic diagram of the essential components of the flow apparatus is shown in Fig. 2. An immersion-type circulating pump was used to supply distilled water (the liquid phase) to the test section. The rate of water supply was controlled by two needle valves, one of which allowed water to by-pass back to the water reservoir and pump system. Another small needle valve was also installed to operate in parallel with the main valve controlling flow into the test section for very fine control of the supply water. The distilled water entered the bottom region of the test section through a disperser connected to the bottom flange. This disperser was basically a vertical copper tube (25.4 mm in diameter) closed at the top with 12 holes (12.7 mm in diameter) distributed over its lateral surface. Thus, the inflow of water was dispersed into 12 horizontal streams to prevent swelling of the gas–liquid interface. The attainment of a smooth interface was essential for an accurate measurement of the liquid height in the test section. The temperature of the water was held steady during the experiment by a cooling coil immersed in the water reservoir, as shown in Fig. 2. The test section was connected to an air supply equipped with a feed-back pressure controller which maintained a steady pressure P_o in the test section throughout the experiment. The test-section pressure, P_o, was monitored by a calibrated pressure gauge. The air flow that entered near the top of the tee-section was also dispersed to maintain a stable, smooth interface.

Details of the geometrical design of the test section were reported by Parrott et al. (1991). Basically, the test section was a large reservoir manufactured from type 304 stainless steel sections, except for a clear acrylic pipe section near the outlet flange for visual observation of the flow phenomena. The outer diameter of this clear acrylic pipe (305 mm) was large enough to prevent visual distortion and its exposed length was 270 mm. Two thermocouples were installed in the test section to sense the temperature of the water and of the air; these thermocouples were mounted in the discharge flange next to the clear acrylic pipe section. All experiments in this investigation were performed at, or near, room-temperature conditions.

The discharge branch was a hole with a diameter $d = 6.35$ mm, machined in a brass block. The brass block, shown in Fig. 3, consisted of two parts: a cylindrical part 104 mm in diameter and 74 mm in length, and a semi-cylindrical part with a diameter of 104 mm and length of 100 mm. The semi-cylindrical section provided a flat plane

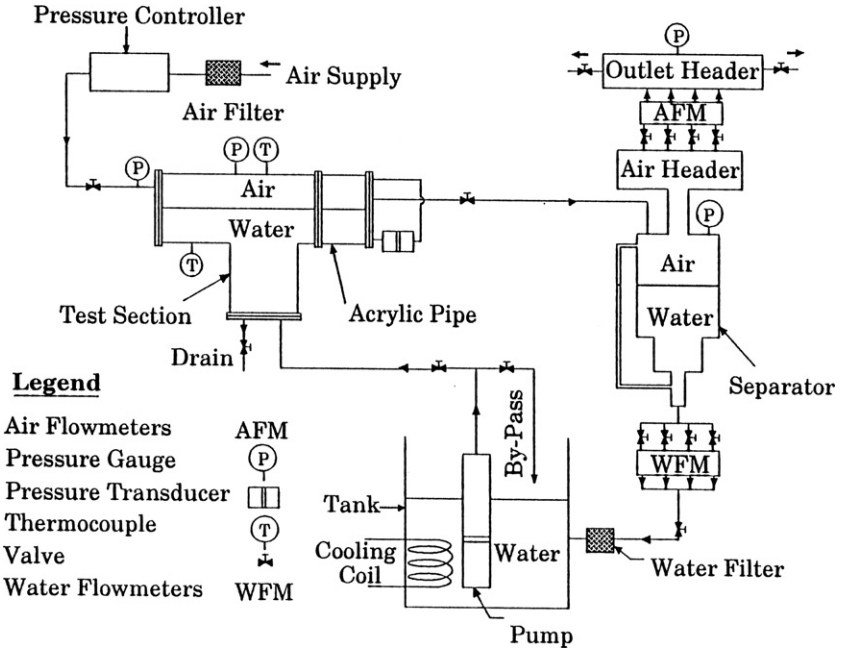

Fig. 2. Schematic of flow loop.

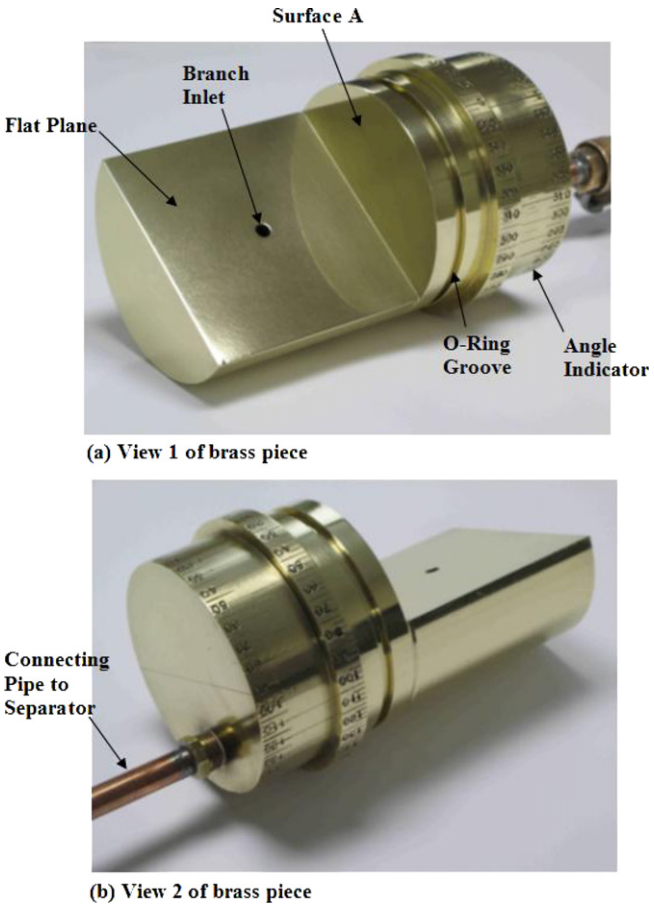

Fig. 3. Views of brass piece.

(104 mm × 100 mm) coincident with the axis of rotation of the cylindrical part. Thus, the outer edge of the branch inlet was at a distance of at least 7.4*d* away from the edges of the flat plane. Rotation of the brass test piece about its centreline gave varying angles of inclination θ of the flat-plane region relative to the vertical direction. The branch hole was machined at the centre of the flat plane, perpendicular to this surface, for a depth of 32 mm (i.e., 5*d*) after which it joined at right angles with another slightly larger-diameter hole that was machined through the whole cylindrical part and half-way through the semi-cylindrical part of the brass piece. This arrangement in the brass piece allowed flow from the test section to downstream components for separating the flow and measuring the rates of flow of both gas and liquid.

The brass piece was mounted and bolted onto the discharge flange of the test section and a seal was made between the brass and flange with an O-ring. After mounting, surface A in Fig. 3 lay in the same plane as the inner surface of the discharge flange. The position where the flat plane of the brass piece was in a vertical position (and the branch centreline was horizontal) became the case of flow through a horizontal branch in a vertical wall ($\theta = 0°$). Angles of rotation of the test piece were accurately marked on the outer circumference of the brass piece (0° to 360°) for setting the angle of inclination of the flat plane. The angle markings were aligned relative to a horizontal reference marking on the outer side of the discharge flange of the test section.

Two pressure taps, one on the air side and the other on the water side, were installed on the outlet flange and connected to a calibrated differential-pressure transducer in order to measure the position of the air–water interface from which the value of h was determined. The air and water were basically at stagnation conditions near these pressure taps and therefore, the dynamic pressure effects on the liquid-level measurement were insignificant. Calibration of the pressure transducer was done at atmospheric pressure to produce a relationship between the height of the water column above a datum and the transducer output voltage. A relationship was available to account for the change in the density of the air from atmospheric conditions to working conditions inside the test section and its effect on sensing the height of the liquid column above a datum during testing (Parrott, 1993).

Locating the centre of the branch entrance in terms of a pressure-transducer voltage was done in order to obtain a reference point for determining the interface height h. It should be noted that locating the branch centre was done for every angle of inclination tested in the present set of experiments even though the test piece rotated about an axis nominally containing the centre of the branch entrance. Theoretically, the branch centre should not change when the test piece is rotated but this would require near-perfect machining of the plane section to the exact centreline of the brass cylinder, in addition to perfectly machining the branch hole in the centre of the plane section. A surveyor's level was used to sight the top or bottom edge (both were done) of the branch; the hair-line was set tangent to the branch circumference. A needle was suspended in the acrylic test section sufficiently away from the test piece (around 8 cm) and was aligned such that the needle tip was at the same elevation as that of the edge of the branch under consideration. Water was allowed to flow into the test section raising the air–water interface until it just touched the tip of the needle; the voltage corresponding to this interface level was then immediately recorded. An average of the transducer voltages obtained in this manner for the top and bottom edges of the branch was calculated and subsequently used to represent the branch centre.

During the experiments, either single-phase air flow or single-phase water flow entered the separation tank, which was maintained at pressure P_s. Flow from the separation tank was directed to a bank of calibrated air rotameters (for the OLE experiments) or a bank of calibrated water rotameters (for the OGE experiments). The air rotameters were capable of measuring flow rates from 19.31 Standard L/min to 1346 Standard L/min. The water rotameters were capable of measuring flow rates from 0.51 to 40.61 L/min. All of the rotameters were of the variable-area type with stainless steel floats. The temperature and pressure of the

air flow through the rotameters were measured using a thermocouple installed just upstream of the rotameter bank and a water manometer connected to the outlet-air header.

2.3. Experimental procedure

The testing program for the OLE and OGE consisted of obtaining the height of the air–water interface, h, at which the onset of entrainment occurred for a range of Froude numbers and for seven angles of inclination of the flat plane of the brass piece relative to the vertical plane (Fig. 1). The angles of inclination that were employed in the experiments were $\theta = 0°$ (vertical plane and horizontal branch), $\theta = 30°$, $\theta = 60°$, $\theta = 90°$ (branch vertically down), $\theta = -30°$, $\theta = -60°$, and $\theta = -90°$ (branch vertically up).

For the OGE experiments, h_{OGE} was measured for a range of liquid Froude number from $Fr_L = 1.5$ to $Fr_L = 70$, all for a fixed value of θ. Similarly, h_{OLE} was measured for a range of gas Froude number from $Fr_G = 1.5$ to $Fr_G = 45$, all for a fixed value of θ. The general procedures that were used to obtain the data are discussed in the following sections.

2.3.1. Liquid-entrainment experiments

These experiments were conducted at a steady test-section pressure $P_o = 317$ kPa. For the chosen angle θ, and with the interface level well below the branch, a steady flow of air was established through the branch at a flow rate that was controlled with a valve just ahead of the air rotameter to give a desired Fr_G. The pressures in the test section, P_o, the separation tank, P_s, and at the exit of the rotameter were recorded. The height of the air–water interface in the test section was gradually increased at a rate of less than 1 mm/min, while the test-section pressure and air flow rate through the branch remained steady. The phenomenon of liquid entrainment into the branch was observed visually through the clear acrylic pipe of the test section and the voltage reading of the pressure transducer was immediately recorded from which the value of h_{OLE} was later calculated.

As the liquid level was increased, the interface deformed in the neighbourhood of the branch. The phenomenon of liquid entrainment observed in this experiment for $\theta \geqslant 0$ for all Fr_G was typically characterized by the sudden formation of a continuous liquid stream from the interface to the branch entrance. For negative inclinations, the phenomenon was characterized by the sudden formation of a continuous liquid stream at low values of Fr_G. At relatively high values of Fr_G with negative inclinations, the phenomena started with entrainment of liquid drops into the branch which intensified as $|h_{OLE}|$ decreased and eventually became a continuous liquid spout. The data reported here for h_{OLE} at any given combination of θ and Fr_G correspond to conditions immediately preceding the formation of a continuous liquid stream or spout.

Following the OLE, the temperature of the air in the test section, T_o, was recorded, and the temperature and pressure of the air at the rotameters were recorded from which the local air density and subsequently, the air mass flow rate, $\dot{m}_G$, were determined. In order to calculate Fr_G, the temperature, pressure, and density of the air at the branch inlet, T_i, P_i, and ρ_i, respectively, were required. This was done by assuming an isentropic expansion of the air from stagnation conditions in the test section (P_o and T_o) to the conditions at the branch inlet (P_i and T_i). Thus,

$$T_i/T_o = (P_i/P_o)^{(k-1)/k}, \tag{2}$$

where k is the ratio of specific heats for air. An energy balance was applied between the stagnation conditions in the test section and the branch inlet assuming ideal gas behaviour, and this resulted in

$$C_p T_o = C_p T_i + 8\left(\frac{\dot{m}_G}{\pi \rho_i d^2}\right)^2, \tag{3}$$

where C_p is the constant-pressure specific heat. The density was calculated from the ideal gas relation as

$$\rho_i = \frac{P_i}{RT_i}, \tag{4}$$

where R is the ideal gas constant for air. Eqs. (2)–(4) were solved iteratively and the converged value of ρ_i was used in Eq. (1) for the calculation of Fr_G.

2.3.2. Gas-entrainment experiments

These experiments were conducted in a manner similar to that described for liquid entrainment except that: in addition to $P_o = 317$ kPa for low Fr_L, $P_o = 520$ kPa was used for high Fr_L; the interface started well *above* the branch with a liquid flow rate for the desired Fr_L; the interface level was *decreased* at the rate of less than 1 mm/min while other conditions remained steady until the onset of gas entrainment was detected by visual observation through the transparent section, thus giving h_{OGE}.

The phenomenon of gas entrainment observed in this experiment was typically characterized by the sudden formation of a gas cone from the interface to the branch entrance. Under certain conditions, such as for higher Fr_L with $\theta = 30°$, $\theta = 60°$, or $\theta = 90°$, a narrow tube of gas extending from the interface to the branch began to appear at high interface levels ($h/d = 3.3$–5.7) and the gas tube persisted as the interface level was lowered. At a certain interface level, this gas tube disappeared and the flow through the branch remained single-phase liquid for a range of h. The appearance of this gas tube was not considered the onset of gas entrainment because the gas flow rates involved were minute and also because the gas tube disappeared as the interface was lowered. With further lowering of the interface level, an intermittent entrainment occurred in which the gas cone was pulled through the branch for a short period of time (~1 s or less). This pattern of intermittent entrainment would persist at times over a range of

interface levels (range of h) until a pattern of continuous gas entrainment was established. For lower Fr_L with $\theta = 30°$, $\theta = 60°$ or $\theta = 90°$, the entrainment pattern was similar to the pattern described above for higher Fr_L, except that the appearance of the narrow gas tube at high h/d did not occur. For a given Fr_L, the values of h at which the different modes of entrainment (the appearance and disappearance of the narrow gas cone, the intermittent entrainment, and the continuous entrainment) occurred were recorded. However, the data reported here for h_{OGE} at any given value of Fr_Lcorrespond to conditions immediately preceding the onset of continuous entrainment.

Following the onset of gas entrainment, the temperatures of the air and water in the test section were recorded for later calculation of the densities ρ_G and ρ_L. The temperature of the water was assumed to remain constant between the test section and the rotameters where the flow rate was read.

2.4. Estimates of experimental uncertainty

An estimate of the uncertainties in the independent and dependent variables was made in the fashion described by Moffat (1988) and Kline and McClintock (1953). All uncertainties quoted here are at "odds" (as used by these authors) of 20 to 1. The uncertainties are meant to accommodate: the accuracy of the calibrating device, the error in fitting an equation (for computer data reduction) to the calibration data, discrimination uncertainties in the measuring instruments, and unsteadiness in the process. Pressure gauges were calibrated using a deadweight tester, thermocouples using a standard mercury-in-glass thermometer, gas rotameters using wet test meters and venturi meters (in turn the calibrations of which are traceable to NIST standards), and liquid rotameters using a weigh-and-time method. The pressure transducer used for measuring h was calibrated against a micro-manometer and the digital voltmeter used in the calibration was subsequently used in the normal running of the experiments; for both calibration and subsequent experiments, the sensitivity of the pressure transducer was approximately 48 mV/mm of water and the discrimination on the digital voltmeter was ±1 mV. The results of the uncertainty analysis are given in Table 1.

Table 1
Measured parameters and their uncertainties

Parameter	Uncertainty
Test-section absolute pressure, P_o	±0.9%
Gas flow rate, $\dot{m}_G$	±4.0%[a]
Liquid flow rate, $\dot{m}_L$	±2.4%[a]
Temperature	±0.25°C
Interface height, h	±0.13 mm[a]
Interface height at OGE, h_{OGE}	±0.16 mm[a]
Interface height at OLE, h_{OLE}	±0.16 mm[a]

[a] Maximum uncertainty.

3. Results and discussion

3.1. Onset of liquid entrainment

A sample of the flow phenomena observed at the OLE is shown in Figs. 4 and 5 for positive and negative values of θ, respectively. In both cases, the Bernoulli effect takes place and it is evidenced at first by a deflection in the interface in the vicinity of the branch entrance. With a further decrease in $|h|$, a stream or spout of water suddenly rises to the branch inlet at the OLE. A key difference between positive and negative angles is that a liquid stream travels along the wall for positive angles, as shown in Fig. 4, while for negative angles, it was possible for a liquid spout to rise directly from the interface to the branch inlet, as shown in Fig. 5. This difference in the flow structure at the onset was found to have a strong influence on the trend of the values of $|h_{OLE}|$.

The experimental data expressed in terms of $|h_{OLE}|/d$ versus Fr_G for $\theta = 0°$, 30°, and 60° are presented in Fig. 6. The data follow a straight line on the log–log scale for all angles. It can be seen that the value of $|h_{OLE}|/d$ decreases as θ increases at the same Fr_G and, as may be expected from physical reasoning, $|h_{OLE}|/d$ should approach zero at $\theta = 90°$ in the absence of surface-tension

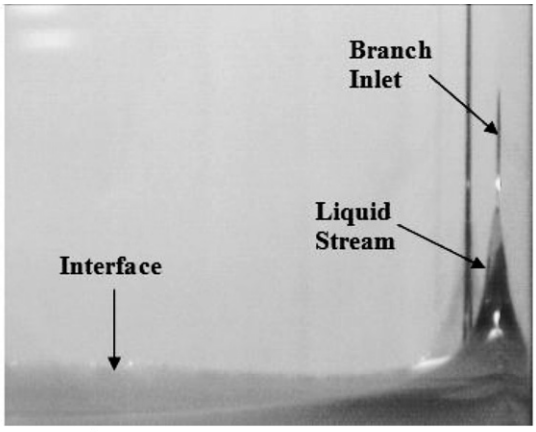

(a) $\theta = 0^o$

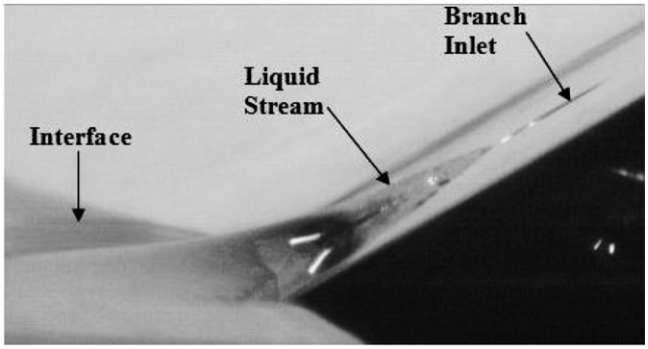

(b) $\theta = 60^o$

Fig. 4. Depiction of the onset of liquid entrainment for $\theta = 0°$ and $\theta = 60°$.

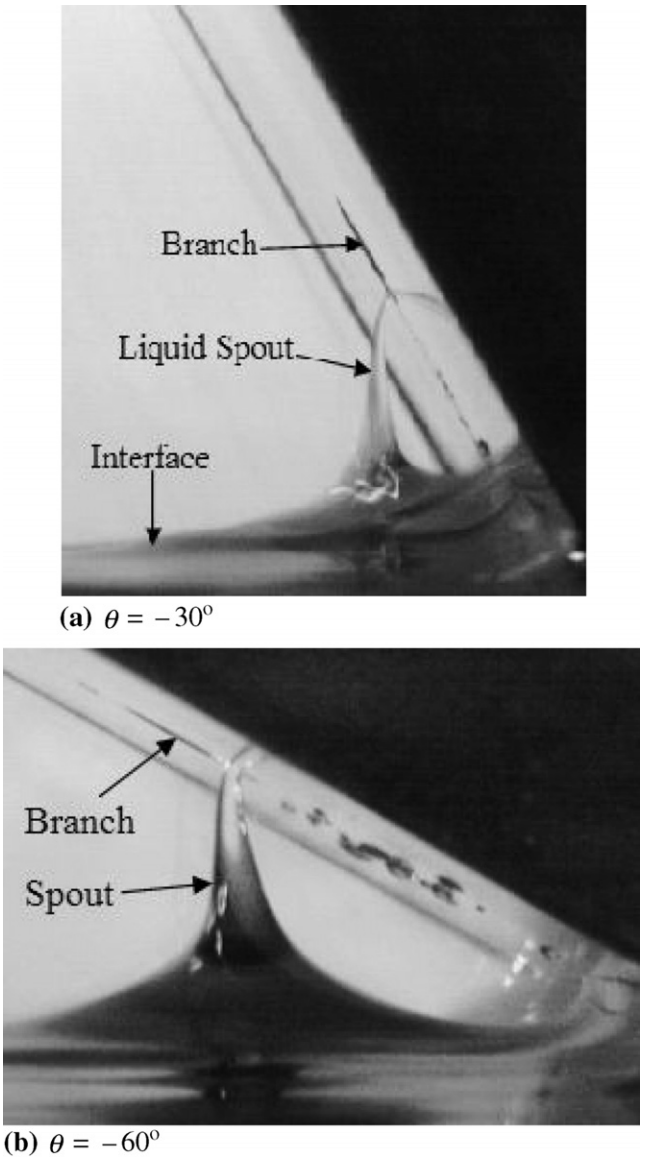

Fig. 5. Depiction of the onset of liquid entrainment for $\theta = -30°$ and $\theta = -60°$.

effects. Also, over the range $0° \leqslant \theta \leqslant 60°$, the slope of the line appears to be increasing with θ.

For $\theta = 0°$, Craya (1949) developed the following theoretical correlation for the OLE at horizontal branches:

$$|h_{OLE}|/d = 0.625 Fr_G^{0.4}. \quad (5)$$

Craya's theory was confirmed experimentally by several authors (e.g., Smoglie and Reimann, 1986; Micaelli and Memponteil, 1989). For correlating the effect of the inclination θ, an equation is sought that reduces to Eq. (5) for $\theta = 0°$, has $|h_{OLE}|/d \to 0$ at $\theta = 90°$, and accommodates the different slopes in the data shown in Fig. 5. Such an equation is

$$|h_{OLE}|/d = [0.625(\cos\theta)^{a_1}] Fr_G^{0.4\left(\cos\frac{\theta}{2}\right)^{a_2}}, \quad 0° \leqslant \theta \leqslant 90°, \quad Fr_G < 45, \quad (6)$$

where a_1 and a_2 are empirical coefficients. Values of a_1 and a_2 that produced the best fit between the data and Eq. (6) were as follows: $a_1 = 1.8$ and $a_2 = -1.8$. In the absence of surface-tension effects, the minimum value of $|h_{OLE}|$ would be $(d/2)\cos\theta$. Therefore, it is suggested as a precaution to limit the use of Eq. (6) to values of Fr_G that result in predicted values of $|h_{OLE}|/d > 0.5\cos\theta$.

A comparison between the experimental data and Eq. (6) is shown in Fig. 6. The deviation between the data and correlation (6) ranges from −7.0% to +6.1% for $\theta = 0°$, from −0.4% to +8.4% for $\theta = 30°$, and from −8.4% to −2.0% for $\theta = 60°$. These values indicate a satisfactory agreement between the data and correlation (6).

Fig. 7 shows the OLE data for the negative angles $\theta = -30°$, $\theta = -60°$, and $\theta = -90°$, together with the data for $\theta = 0°$. Craya's (1949) correlation, given by Eq. (5), and lines of ±20% deviation from the correlation are also shown in the figure. It can be observed that nearly all data points in Fig. 7 fall within the ±20% bounds of Eq. (5). This trend is consistent with the flow phenomena shown earlier in Fig. 5 for negative angles, where the liquid spout that formed at the onset travelled directly from the

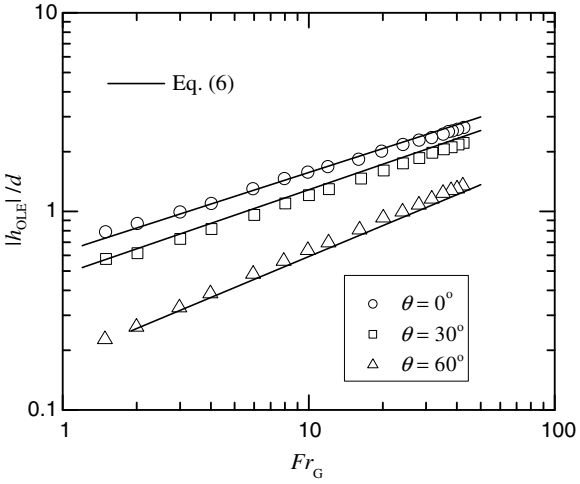

Fig. 6. The onset of liquid entrainment for positive θ.

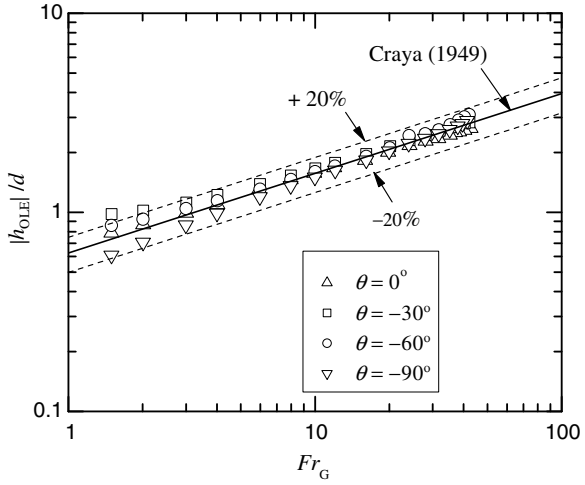

Fig. 7. The onset of liquid entrainment for negative θ.

interface to the branch inlet. Because of that, the value of $|h_{OLE}|$ was not influenced significantly by the inclination of the wall, and so was different from the case with positive θ where the liquid stream travelled along the wall.

For the case of a top branch ($\theta = -90°$), several previous investigations proposed a correlation of the following form for the OLE:

$$|h_{OLE}|/d = C_1 Fr_G^{C_2}. \quad (7)$$

However, there has been considerable disagreement among authors on the values of C_1 and C_2, as shown in Table 2. Smoglie and Reimann (1986) obtained empirical values of C_1 and C_2 for high-pressure air–water data, Schrock et al. (1986) reported values for high-pressure steam-water data, while Micaelli and Memponteil (1989) obtained values for C_1 and C_2 using data from different sources (including Smoglie and Reimann, and Schrock et al.). Micaelli and Memponteil noted significant scattering in the data particularly in the region $|h_{OLE}|/d < 4$, where all of the present data lie, and they attributed this scatter to the difficulty in detecting the onset for the test-section configuration used in the experiments and also due to fluctuations in the flow field. In the present experiment, the liquid pool was stagnant and the interface was smooth (no disturbance discernible by naked eye) away from onset location. The present data for $\theta = -90°$ agree best with the empirical correlation of Rouse et al. (1956) who obtained $C_1 = 0.536$ and $C_2 = 0.4$ under experimental conditions similar to the present ones.

Table 2
Values of C_1 and C_2 in Eq. (7)

Source	C_1	C_2
Smoglie and Reimann (1986)	1.52	0.4
Schrock et al. (1986)	1.45	0.4
Micaelli and Memponteil (1989)	0.596	0.67
Rouse et al. (1956)	0.536	0.4

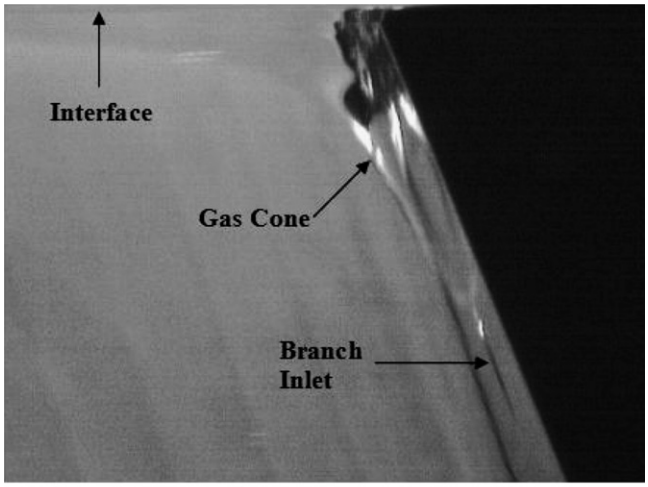

(a) $\theta = -30°$

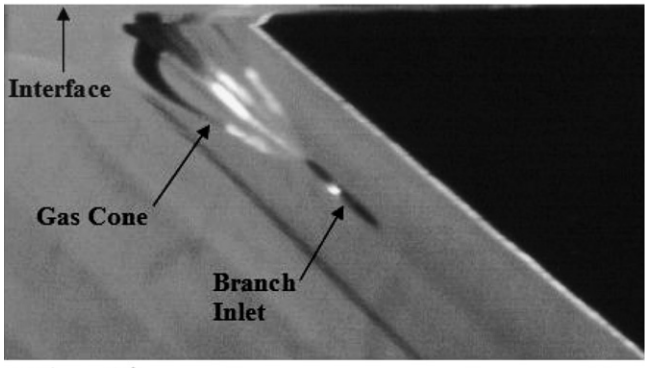

(b) $\theta = -60°$

Fig. 8. Depiction of the onset of gas entrainment for $\theta = -30°$ and $\theta = -60°$.

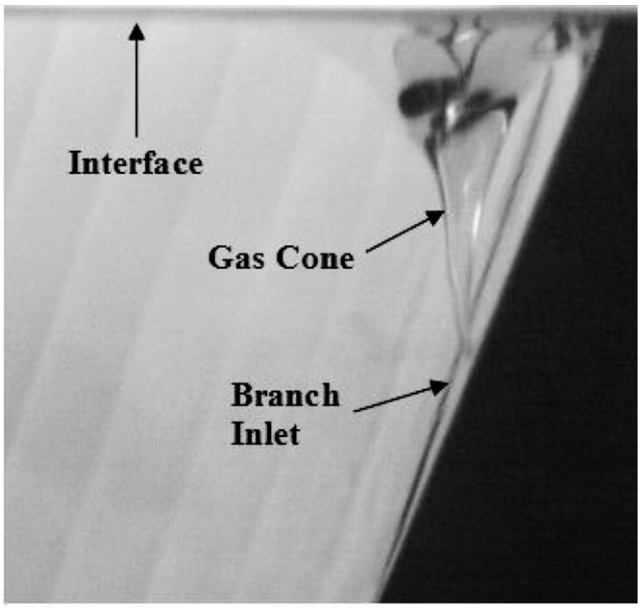

(a) $\theta = 30°$

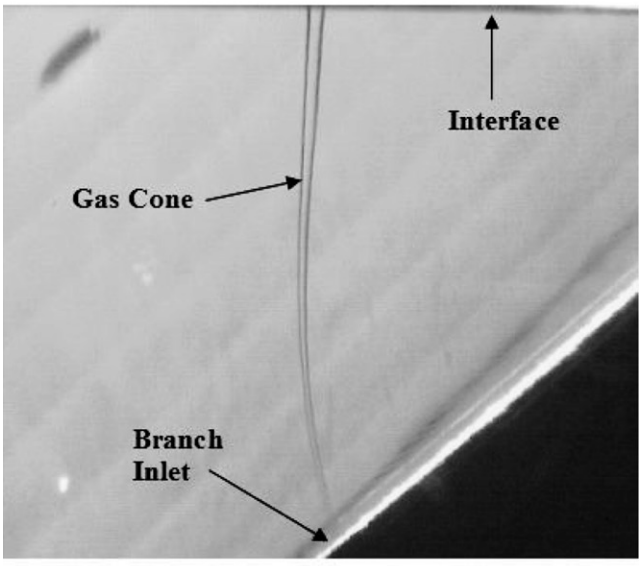

(b) $\theta = 60°$

Fig. 9. Depiction of the onset of gas entrainment for $\theta = 30°$ and $\theta = 60°$.

3.2. Onset of gas entrainment

The phenomenon of gas entrainment at various wall inclinations was found to be almost the mirror image of the phenomenon of liquid entrainment. Figs. 8 and 9 show photographs of the gas cone that forms at the onset for negative and positive values of θ, respectively. A dip forms at the interface in all cases just prior to the onset. It can be seen from Figs. 8 and 9 that the gas cone for positive angles θ stretches directly from the interface to the branch without touching the wall, while for negative θ, parts of the gas cone appear to touch the wall. For that reason, the value of h_{OGE} at positive angles θ was found to be nearly independent of θ, as will be shown later.

The OGE data are shown in Figs. 10 and 11 for negative and positive θ, respectively. Fig. 10 shows the data for angles $\theta = 0°$, $\theta = -30°$, and $\theta = -60°$; for $\theta = -90°$, in the absence of surface-tension effects, h_{OGE} approaches zero for all values of Fr_L based on physical reasoning. Also, in the absence of surface-tension effects, h_{OGE}/d should approach $0.5\cos\theta$ as Fr_L approaches zero. The data are presented in a semi-log plot because h_{OGE} becomes negative for $\theta = -60°$ and low values of Fr_L. It may be noted also that h_{OGE}/d reaches values lower than $0.5\cos\theta$ for $\theta = -30°$ and low values of Fr_L. The reason for both of these conditions is that the surface tension force becomes significant at low liquid flow rates whereby a liquid meniscus forms at the top edge of the branch opening and the liquid flow is not strong enough to tear the meniscus off the branch opening.

In correlating the data, it was assumed that inertia and gravity forces are the dominant forces involved in the onset phenomenon, thus neglecting surface tension which is expected to be significant only at low Fr_L. Therefore, a correlation in the form of Eq. (7) was sought for the data of $\theta = 0°$ and the line of best fit was found to be

$$h_{OGE}/d = 0.475 Fr_L^{0.444}. \tag{8}$$

The deviation between Eq. (8) and the data for $\theta = 0°$ ranged from −6.0% to +1.73%. Previous researchers also used

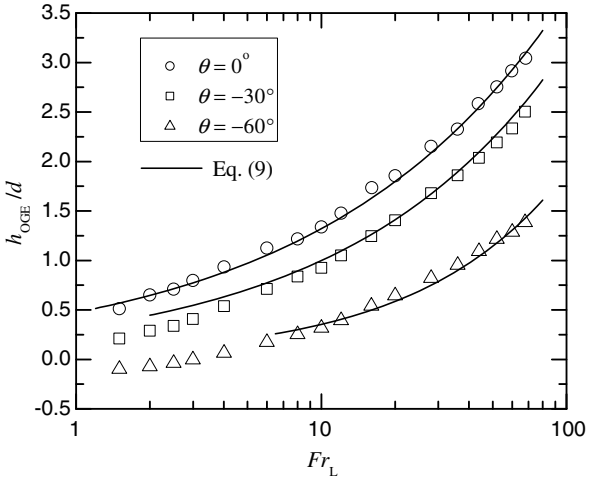

Fig. 10. The onset of gas entrainment for negative θ.

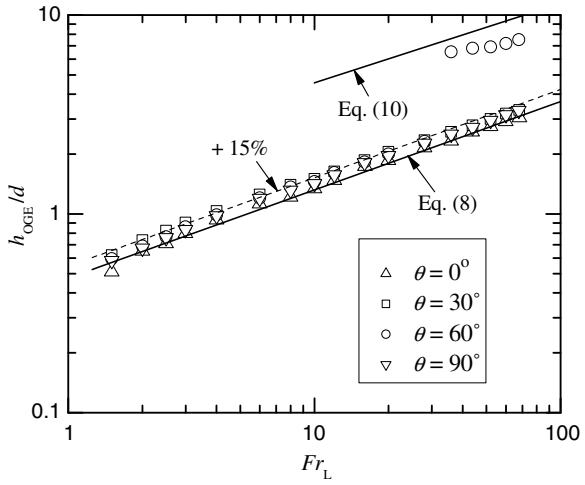

Fig. 11. The onset of gas entrainment for positive θ.

the form of Eq. (8) in correlating the OGE data for horizontal branches. Smoglie and Reimann (1986) obtained 0.68 for the coefficient and 0.4 for the exponent, while Micaelli and Memponteil (1989) produced 0.625 for the coefficient and 0.4 for the exponent.

A correlating equation that includes the effect of inclination and reduces to Eq. (8) at $\theta = 0°$ and $h_{OGE}/d = 0$ at $\theta = -90°$ is proposed as

$$h_{OGE}/d = [0.475(\cos\theta)^{b_1}]Fr_L^{0.444\left(\cos\frac{\theta}{2}\right)^{b_2}}, \quad -90° \leqslant \theta \leqslant 0°, \quad Fr_L < 70, \tag{9}$$

where b_1 and b_2 are empirical coefficients. A best fit with the data of $\theta = -30°$ and $\theta = -60°$ was obtained with $b_1 = 2.85$ and $b_2 = -3.45$. The deviations between the data and correlation (9) range from −0.5% to +8.8% at $\theta = -30°$ and from −9.1% to +11.5% at $\theta = -60°$. These deviations do not include the data affected by surface tension. Eq. (9) should only be used with values of Fr_L that result in predicted values of $h_{OGE}/d > 0.5\cos\theta$.

The OGE data for $\theta = 30°$, 60°, and 90° are presented in Fig. 11. The figure shows that the data for all positive angles, together with the data for $\theta = 0°$, collapsed in a narrow band bounded by Eq. (8) and a line 15% higher than the line from Eq. (8). This trend is consistent with the way by which the gas cone formed, namely without touching the wall, as discussed earlier. For $\theta = 60°$ and $Fr_L > 30$, continuous gas entrainment was observed by what appeared to be a vortex flow. The gas flow corresponding to all other data points in Figs. 10 and 11 appeared to be vortex free. The vortex-flow data points in Fig. 11 correspond to significantly higher values of h_{OGE}/d. For downward branches (i.e., $\theta = 90°$), Smoglie and Reimann (1986) proposed the following correlation for the onset of gas entrainment:

$$h_{OGE}/d = K Fr_L^{0.4}, \tag{10}$$

with $K = 0.625$ for vortex-free entrainment and $K = 1.816$ for vortex entrainment. Eq. (10) with $K = 1.816$ is shown in Fig. 11 and it appears to be close to the present vortex-entrainment data.

3.3. Comparison with Lee et al. (2007)

Since the work of Lee et al. (2007) is the only other published study on the onsets of gas and liquid entrainment from inclined branches, it is important to compare the present results with those of Lee et al. It must be pointed out however that there is a major difference in the geometry considered in both studies whereby Lee et al. considered inclined branches mounted on a circular header while the present study considered inclined branches mounted on a flat wall. This difference in geometry may have had an influence on the magnitude and trends of the results.

For the onset of liquid entrainment, Lee et al. considered branch inclinations of $\theta = 0°$, $-30°$, $-45°$, $-60°$, and $-90°$, and their data were mostly in the range $1 \leqslant Fr_G \leqslant 10$. For these conditions, Lee et al. reported that the value of $|h_{OLE}|/d$ was significantly affected by the inclination angle θ, that this effect decreased as Fr_G increased, and they predicted that the effect would be insignificant for $Fr_G > 10$. On the other hand, the present data of OLE considered branch inclinations of $\theta = 0°$, $\pm 30°$, $\pm 60°$, and $-90°$, and a Froude-number range of $1 \leqslant Fr_G \leqslant 45$. For the negative angles, which were considered by Lee et al., the present results showed a small effect of θ on $|h_{OLE}|/d$ over the whole range of Fr_G, as shown in Fig. 7. However, for positive θ, significant effects of θ on $|h_{OLE}|/d$ were noted in the present study (see Fig. 6), while the study by Lee et al. did not include positive values of θ for the OLE.

For the onset of gas entrainment, Lee et al. considered branch inclinations of $\theta = 0°$, $30°$, $45°$, $60°$, and $90°$, and their data were mostly in the range $2 \leqslant Fr_L \leqslant 30$. Similarly, for these conditions, Lee et al. noted that the value of h_{OGE}/d was affected by θ, that this effect decreased as Fr_L increased, and they predicted that the effect would be insignificant for $Fr_L > 10$. On the other hand, the present data of OGE considered branch inclinations of $\theta = 0°$, $\pm 30°$, $\pm 60°$, and $90°$, and a Froude-number range of $1 \leqslant Fr_L \leqslant 70$. For the positive angles, which were considered by Lee et al., the present results showed a small effect of θ on h_{OGE}/d over the whole range of Fr_L, as shown in Fig. 11. However, for negative θ, significant effects of θ on h_{OGE}/d were noted in the present study (see Fig. 10), while the study by Lee et al. did not include negative values of θ for the OGE. These observations about the findings of Lee et al. relative to those of the present study underline the need for further research on this topic.

4. Conclusions

New experimental data are reported for the onsets of liquid and gas entrainment for discharge through a circular outlet branch in a flat plane at various angles of inclination. The following conclusions can be drawn from the results of this investigation:

1. For negative θ, $|h_{OLE}|/d$ is essentially independent of θ for a given Fr_G.
2. For positive θ, $|h_{OLE}|/d$ is correlated empirically in terms of Fr_G and θ; good agreement is seen between the experimental data and the correlation.
3. For positive θ, h_{OGE}/d is essentially independent of θ for a given Fr_L.
4. For negative θ, h_{OGE}/d is correlated empirically in terms of Fr_L and θ; good agreement is seen between the experimental data and the correlation.
5. For the cases where the onset h/d was essentially independent of θ, these were explained in terms of the physical appearance of the entrainment process.

Acknowledgement

Funding provided by the Natural Sciences and Engineering Research Council of Canada (NSERC) is gratefully acknowledged.

References

Craya, A., 1949. Theoretical research on the flow of non-homogeneous fluids. Houille Blanche 4, 44–55.

Hassan, I.G., Soliman, H.M., Sims, G.E., Kowalski, J.E., 1998. Two-phase flow from a stratified region through a small side branch. ASME J. Fluids Eng. 120, 605–612.

Kline, S.J., McClintock, F.A., 1953. Describing the uncertainties in single-sample experiments. Mech. Eng. J. 75, 3–8.

Lee, J.Y., Hwang, S.H., Kim, M., Park, G.C., 2007. Onset condition of gas and liquid entrainment at an inclined branch pipe on a horizontal header. Nucl. Eng. Des. 237, 1046–1054.

Micaelli, J.C., Memponteil, A., 1989. Two-phase flow behaviour in a tee-junction: the CATHARE model. In: Proceedings of the Fourth International Topical Meeting on Nuclear Reactor Thermal-Hydraulics, Karlsruhe, Germany, vol. 2, pp. 1024–1030.

Moffat, R.J., 1988. Describing the uncertainties in experimental results. Exp. Thermal Fluid Sci. 1, 3–17.

Parrott, S.D., 1993. Experiments on the onsets of gas pull-through and liquid entrainment during dual discharge from a large reservoir, M.Sc. Thesis, University of Manitoba, Winnipeg, Canada.

Parrott, S.D., Soliman, H.M., Sims, G.E., Krishnan, V.S., 1991. Experiments on the onset of gas pull-through during dual discharge from a reservoir. Int. J. Multiphase Flow 17, 119–129.

Reimann, J., Khan, M., 1984. Flow through a small break at the bottom of a large pipe with stratified flow. Nucl. Sci. Eng. 88, 297–310.

Rouse, H., Davidian, J., Glover, J.E., Appel, D.W., 1956. Development of the non-circulatory waterspout. ASCE J. Hydraul. Div. 82, 1038(3)–1038(7).

Schrock, V.E., Revankar, S.T., Mannheimer, R., Wang, C.H., Jia, D., 1986. Steam-water critical flow through small pipes from stratified upstream regions. In: Proceedings of the Eighth International Heat Transfer Conference, San Francisco, CA, vol. 5, pp. 2307–2311.

Smoglie, C., Reimann, J., 1986. Two-phase flow through small branches in a horizontal pipe with stratified flow. Int. J. Multiphase Flow 12, 609–625.

Welter, K.B., Wu, Q., You, Y., Abel, K., McCreary, D., Bajorek, S.M., Reyes Jr, J.N., 2004. Experimental investigation and theoretical

modeling of liquid entrainment in a horizontal tee with a vertical-up branch. Int. J. Multiphase Flow 30, 1451–1484.

Yonomoto, T., Tasaka, K., 1988. New theoretical model for two-phase flow discharged from stratified two-phase region through small break. J. Nucl. Sci. Technol. 25, 441–455.

Yonomoto, T., Tasaka, K., 1991. Liquid and gas entrainment to a small break hole from a stratified two-phase region. Int. J. Multiphase Flow 17, 745–765.

Zuber, N., 1980. Problems in modelling of small break LOCA. Nuclear Regulatory Commission Report, NUREG-0724.